Salt-inducible kinase 1 maintains HDAC7 stability to promote pathologic cardiac remodeling

Austin Hsu,[1,2,3] Qiming Duan,[3] Sarah McMahon,[1,3] Yu Huang,[3] Sarah A.B. Wood,[2,3] Nathanael S. Gray,[4,5] Biao Wang,[6] Benoit G. Bruneau,[2,3,6,7] and Saptarsi M. Haldar[3,6,8]

[1]Biomedical Sciences Graduate Program, UCSF, San Francisco, California, USA. [2]Gladstone Institutes, San Francisco, California, USA. [3]Roddenberry Center for Stem Cell Biology and Medicine, Gladstone Institutes, San Francisco, California, USA. [4]Department of Cancer Biology, Dana-Farber Cancer Institute, Boston, Massachusetts, USA. [5]Department of Biological Chemistry and Molecular Pharmacology, Harvard Medical School, Boston, Massachusetts, USA. [6]Cardiovascular Research Institute, [7]Department of Pediatrics, and [8]Cardiology Division, Department of Medicine, UCSF, San Francisco, California, USA.

Salt-inducible kinases (SIKs) are key regulators of cellular metabolism and growth, but their role in cardiomyocyte plasticity and heart failure pathogenesis remains unknown. Here, we showed that loss of SIK1 kinase activity protected against adverse cardiac remodeling and heart failure pathogenesis in rodent models and cardiomyocytes derived from human induced pluripotent stem cells. We found that SIK1 phosphorylated and stabilized histone deacetylase 7 (HDAC7) protein during cardiac stress, an event that is required for pathologic cardiomyocyte remodeling. Gain- and loss-of-function studies of HDAC7 in cultured cardiomyocytes implicated HDAC7 as a prohypertrophic signaling effector that can induce *c-Myc* expression, indicating a functional departure from the canonical MEF2 corepressor function of class IIa HDACs. Taken together, our findings reveal what we believe to be a previously unrecognized role for a SIK1/HDAC7 axis in regulating cardiac stress responses and implicate this pathway as a potential target in human heart failure.

Introduction

In response to cardiac insults, the heart undergoes stress-dependent pathologic remodeling, a process that features hypertrophic cardiomyocyte growth and transcriptional activation of a gene program that can chronically compromise cardiac function (1). A major regulator of stimulus-coupled transcription in cardiomyocytes is the class IIa histone deacetylase (HDAC) protein family (HDAC4, HDAC5, HDAC7, HDAC9), which lack significant catalytic activity and are generally thought to function as potent allosteric corepressors of MEF2 transcriptional activity (2). In response to stress signals, a subset of intracellular kinases directly interact with class IIa HDACs and phosphorylate them on specific, conserved serine residues — an event that promotes nuclear export of these HDACs and consequent derepression of MEF2 transcriptional function. Consistent with this model, genetic deficiency of HDAC4, HDAC5, or HDAC9 is each associated with excessive myocardial MEF2 activity and heart failure in mice (2–4). In this manner, phosphorylation of class IIa HDACs by specific kinases (e.g., CaMKII, PKD) functions as a signal-responsive mechanism that directly couples cytosolic stress signaling cascades with the nuclear gene control machinery. Therefore, identification of upstream kinases that regulate HDACs in the heart is essential for our mechanistic understanding of cardiac stress responses, knowledge that may inform novel therapeutic strategies for human heart failure.

Salt-inducible kinases (SIKs; SIK1, SIK2, SIK3 in mammals) are a family of serine/threonine protein kinases that have been shown to regulate skeletal muscle homeostasis and the hepatic fasting response by modulating HDAC4 and HDAC5 function (5, 6). However, the role of SIKs in the heart is largely unknown. In this study, we establish SIK1 as an essential positive regulator of pathologic cardiac remodeling. Leveraging complementary gene-specific siRNA knockdown and chemical inhibition approaches, we demonstrate that inhibition of SIK1 blocks cardinal features of pathologic remodeling in vitro. Similarly, global SIK1-deficient mice are protected from pressure overload–induced heart failure. Mechanistically, we uncover HDAC7 as a major downstream target of SIK1 phosphorylation and demonstrate that loss of this phosphorylation event leads to proteasome-mediated degradation of HDAC7. Specific siRNA-mediated knockdown of *Hdac7* in cultured cardiomyocytes reveals that it functions as a positive regulator of cardiomyocyte hypertrophy and stress-gene transactivation. This mechanism represents a function that is distinct from that of HDAC4, HDAC5, or HDAC9, which act as MEF2 corepressors and negative regulators of cardiomyocyte hypertrophy and heart failure pathogenesis. In addition, we find that HDAC7 activates *c-Myc*, a well-established transcriptional driver of cardiomyocyte stress responses (7, 8), further supporting a distinct mechanism of

▶ **Related Commentary: https://doi.org/10.1172/JCI137074**

Authorship note: BGB and SMH contributed equally to this work.
Conflict of interest: BGB is a cofounder of, consultant to, and shareholder in Tenaya Therapeutics. SMH is an executive and officer of and shareholder in Amgen. SMH is a cofounder of and shareholder in Tenaya Therapeutics. NSG is a founder and science advisory board member of and equity holder in Gatekeeper, Syros, Petra, C4 Therapeutics, B2S Life Sciences, and Soltego. The Gray laboratory receives or has received research funding from Novartis, Takeda, Astellas, Taiho, Janssen, Kinogen, Voronoi, Her2llc, Deerfield, and Sanofi.
Copyright: © 2020, American Society for Clinical Investigation.
Submitted: September 24, 2019; **Accepted:** February 20, 2020; **Published:** May 4, 2020.
Reference information: *J Clin Invest*. https://doi.org/10.1172/JCI133753.

action for HDAC7 compared with other class IIa HDACs. Taken together, these findings identify SIK1 as a critical effector of cardiomyocyte stress responses and heart failure pathogenesis and implicate HDAC7 as a major downstream target of SIK1 signaling during cardiomyocyte hypertrophy.

Results

Pan-SIK inhibition attenuates hallmark features of pathologic cardiomyocyte remodeling in vitro. To our knowledge, the role of SIKs in heart failure has not been previously explored. As SIKs have been implicated as a link between cytosolic signaling cascades and the nuclear gene control machinery in hepatocyte metabolic adaptation (6), we hypothesized that this family of kinases might regulate cardiomyocyte plasticity during heart failure–related stress. We began by testing whether broad inhibition of all 3 SIK isoforms would have any effect on the cardiomyocyte stress response. We leveraged the neonatal rat ventricular myocyte (NRVM) cell culture model, which has been well established to mount a stereotypic response to hypertrophic stimuli such as phenylephrine (PE), featuring an increase in cell size (hypertrophy) and activation of a heart failure–related gene expression program (9). We tested the effect of 2 structurally distinct, potent, and relatively specific chemical inhibitors of the SIK family (HG-9-91-01) and YKL-05-099) (10) on NRVMs treated with and without PE. Treatment with either SIK inhibitor potently attenuated hallmark features of pathologic cardiomyocyte remodeling in a dose-dependent manner, including cellular hypertrophy (Figure 1, A and B) and induction of canonical heart failure–associated marker genes such as *Nppa*, *Nppb*, *Ctgf*, and *Il6* (refs. 11, 12; Figure 1C; and Supplemental Figure 1A; supplemental material available online with this article; https://doi.org/10.1172/JCI133753DS1). The effects of these inhibitors on cardiomyocyte hypertrophy and gene expression in the baseline state are shown in Supplemental Figure 1, B–E. To provide human relevance to our findings, we tested the effects of SIK inhibitors in an established model of endothelin-1–induced (ET-1–induced) hypertrophy in cardiomyocytes derived from human induced pluripotent stem cells (iPSCs) (13). Treatment with either SIK inhibitor suppressed ET-1–induced cellular hypertrophy, upregulation of *NPPB* mRNA, and secretion of proBNP protein into the medium, in a dose-dependent manner (Figure 1, D–F).

SIK1 is a positive regulator of pathologic cardiomyocyte remodeling in vitro. Pan-SIK chemical probes, such as YKL-05-099, also have activity against Src kinases and cannot discriminate which SIK isoform is critical for driving cardiomyocyte hypertrophy (10). We therefore used gene-specific siRNAs in our NRVM system to assess which SIK isoforms might be mediating the prohypertrophic effect. Three mammalian SIK isoforms have been identified to date: SIK1, SIK2, and SIK3 (14). In NRVMs, we were unable to detect *Sik2* transcripts by quantitative reverse transcription PCR (qRT-PCR) at baseline or after PE stimulation. *Sik1* transcripts were readily detected and strongly induced by PE stimulation, suggesting that SIK1 may play a role in the early cardiac stress response. *Sik3* transcripts were also detected in NRVMs but did not change with PE stimulation (Figure 2A). We used specific siRNA probes to knock down *Sik1* or *Sik3* in NRVMs and assayed for the effect of knockdown on cardiac hypertrophy. *Sik1* knockdown had no appreciable effect on cardiac myocytes under basal conditions, but potently attenuated PE-induced hypertrophy and gene induction (Figure 2, B–D, and Supplemental Figure 2, A and B). In contrast, knockdown of *Sik3* induced spontaneous hypertrophy and activation of heart failure–associated genes under basal conditions and further exacerbated the PE-induced stress response (Figure 2, B, C, and E, Supplemental Figure 2, A and B, and Supplemental Figure 4D). Taken together, these data demonstrate that SIK1 is the specific isoform that positively regulates cardiomyocyte hypertrophy and stress-gene activation.

Global loss of SIK1 protects against pathologic cardiac remodeling in vivo. Prompted by these observations in cultured NRVMs, we hypothesized that SIK1 would also be required for pathologic cardiac remodeling and heart failure pathogenesis in vivo. Global *Sik1*$^{-/-}$ mice (15) and WT littermate controls were subject to cardiac pressure overload by transverse aortic constriction (TAC) (16). After 6 weeks of TAC, *Sik1*$^{-/-}$ mice had less cardiomegaly and cardiac hypertrophy (Figure 3, A and B, and Supplemental Figure 2C). Serial echocardiography demonstrated that *Sik1* deficiency attenuated the progressive decline in left ventricular (LV) systolic dysfunction seen in WT mice (Figure 3C). In addition, *Sik1*$^{-/-}$ mice exhibited attenuated features of heart failure, such as reduced LV fibrosis (Figure 3D), reduced cardiomyocyte hypertrophy (Figure 3E), and blunted induction of stereotypical heart failure–related genes (Figure 3F). *Sik1* deficiency did not alter cardiac structure or function in the sham-treated group (Figure 3C). These data implicate SIK1 as a critical regulator of stress-induced pathologic cardiac remodeling and heart failure progression in vivo.

HDAC7 stability is dependent on SIK1 kinase activity. In other cellular contexts, SIK1 has been shown to phosphorylate and regulate HDAC4 and HDAC5 (5, 6). To test whether SIK1 targets class IIa HDACs in cardiomyocytes, we harvested whole-cell lysates from NRVMs treated with *Sik1* siRNA with or without PE and performed Western blot analysis using a phospho-specific antibody that can discriminate orthologous phosphorylation status of HDAC4 (serine 246), HDAC5 (serine 259), and HDAC7 (serine 155). *Sik1* knockdown did not significantly affect phospho-HDAC4 or phospho-HDAC5 abundance in NRVMs (Figure 4A). However, phospho-HDAC7 abundance was significantly depleted with *Sik1* knockdown. We assessed total protein abundance of class IIa HDAC isoforms and found that total HDAC7 protein abundance was robustly and specifically decreased with *Sik1* knockdown, implicating an unexpected role for SIK1 in maintaining total HDAC7 protein concentration (Figure 4A). *Hdac7* transcript levels remained unchanged in the setting of *Sik1* knockdown (Figure 4B), indicating that SIK1-mediated regulation of HDAC7 occurs in a post-transcriptional manner. To test whether this mode of regulation is dependent on the intrinsic kinase activity of SIK1, we performed Western blot analysis on NRVMs treated with the pan-SIK chemical inhibitors HG-9-91 and YKL-05-099. Both inhibitors phenocopied the effects of the *Sik1* siRNA on HDAC7, depleting total and phosphorylated HDAC7 abundance under both baseline and PE-stimulated conditions (Figure 4, C and D). Furthermore, Western blot analysis on cardiac tissue samples from global *Sik1*$^{-/-}$ mice also revealed decreased total and phosphorylated HDAC7 protein at baseline and after TAC (Figure 4E), demonstrating that this SIK1/HDAC7 axis is preserved in vivo and across species. The effect of SIK1 deficiency on HDAC7 protein abundance was less

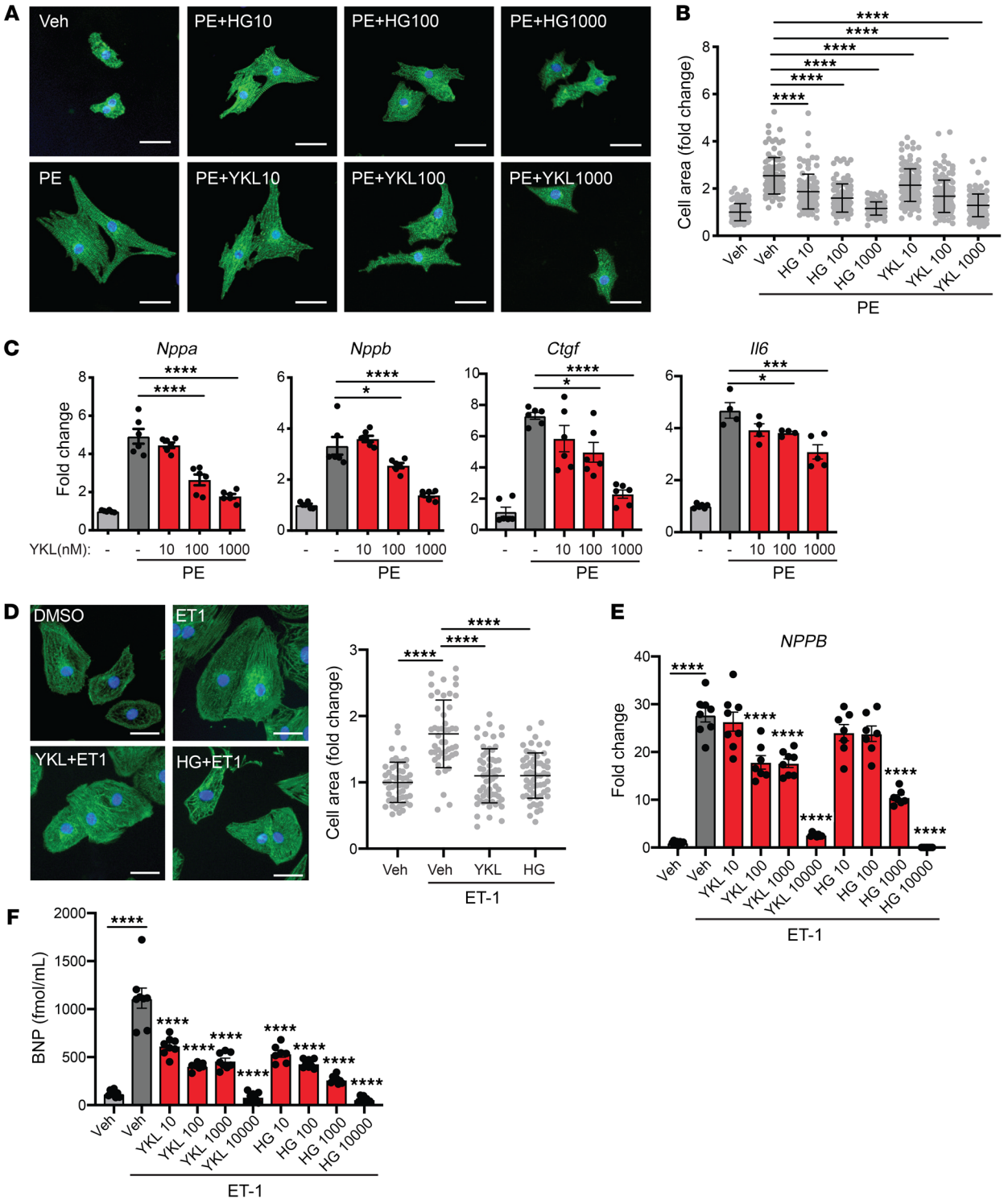

Figure 1. Pan-SIK inhibitors attenuate hallmark features of cardiomyocyte hypertrophy in vitro. (**A**) NRVMs immunostained for α-actinin (green) and nuclei (blue). Scale bars: 40 μm. (**B**) Cell area of NRVMs treated with 100 μM phenylephrine (PE) for 48 hours with or without pan-SIK small-molecule inhibitors HG-9-91-01 (HG) and YKL-05-099 (YKL) (nanomolar concentrations) (n = 100–130). Bars denote mean ± SD. (**C**) qRT-PCR expression for canonical heart failure–associated genes (n = 4–6). (**D**) iPSC cardiomyocytes (CMs) immunostained for α-actinin (green) and nuclei (blue) (n = 48–59). Scale bars: 40 μm. (**E**) qRT-PCR expression of *NPPB* in iPSC-CMs (n = 7–8). (**F**) ELISA for proBNP protein secretion into culture medium of iPSC-CMs (n = 7–8). Data are shown as means ± SEM unless noted. *P < 0.05, ***P < 0.001, ****P < 0.0001 by 1-way ANOVA with Tukey's multiple comparisons test.

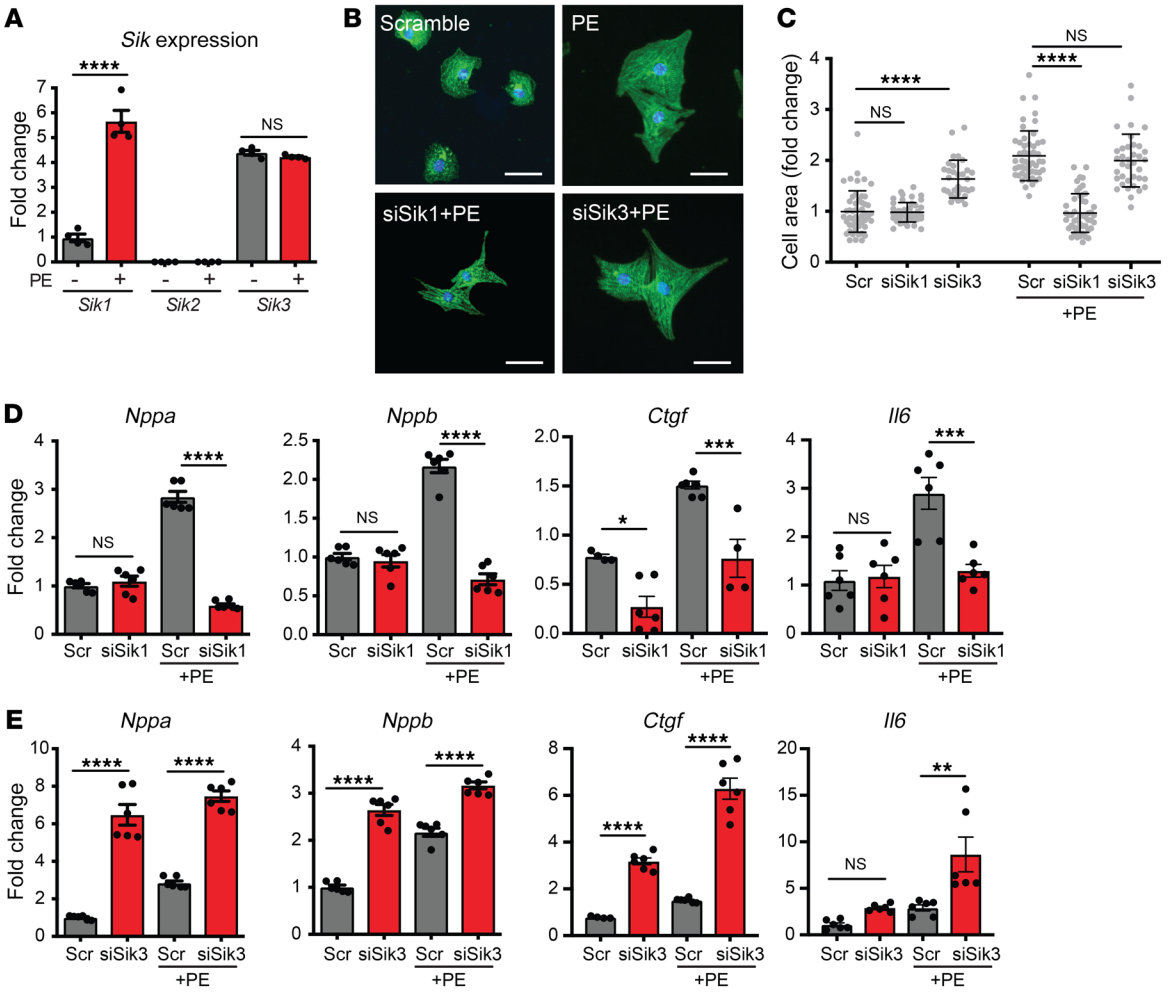

Figure 2. SIK1 is a positive regulator of cardiomyocyte hypertrophy. (**A**) qRT-PCR expression of *Sik* transcripts in NRVMs treated with or without PE (100 μM, 48 hours) (n = 4). (**B**) NRVMs treated with siRNAs against *Sik1* or *Sik3* and immunostained for α-actinin (green) and nuclei (blue). Scale bars: 40 μm. (**C**) Cell area of NRVMs (n = 30–50). Bars denote mean ± SD. (**D** and **E**) qRT-PCR expression for canonical heart failure–associated genes (n = 4–6). Data are shown as means ± SEM unless noted. *P < 0.05, **P < 0.01, ***P < 0.001, ****P < 0.0001, by 1-way ANOVA with Tukey's multiple comparisons test.

pronounced in the TAC-treated group compared with the sham group, suggesting that pressure overload may induce the expression or activity of additional kinases or alternative mechanisms that can modulate HDAC7 stability in the adult mouse heart.

To further test whether this effect was due to a direct kinase-substrate interaction between SIK1 and HDAC7, we performed an in vitro kinase assay using recombinant SIK1 and HDAC7 protein. As expected, HDAC7 alone did not exhibit basal phosphorylation signal. However, addition of both SIK1 and HDAC7 induced phosphorylation of Ser155, which was lost upon addition of the SIK inhibitor YKL-05-099 (Figure 4F). We also found that SIK1 could phosphorylate Ser318 and Ser488 in this assay, 2 residues that have been implicated in the interaction of HDAC7 with 14-3-3 (Supplemental Figure 2D and ref. 17). This evidence supporting a direct kinase-substrate interaction led us to hypothesize that loss of SIK1 kinase activity decreases phosphorylation of HDAC7, leading to proteasome-mediated HDAC7 degradation. Consistent with this hypothesis, treating NRVMs with the proteasome inhibitor bortezomib rescued the SIK inhibitor–dependent depletion of HDAC7 protein (Figure 4G). In addition, treatment of NRVMs with the SIK inhibitor YKL-05-099 increased the ratio of ubiquitinated HDAC7 to total HDAC7 (Supplemental Figure 4, A and B). Bortezomib also led to a relative increase in the ubiquitinated HDAC7/total HDAC7 ratio compared with baseline, although this ratio was not further augmented by YKL-05-099 cotreatment, possibly because potent proteasome inhibition by itself may lead to saturating levels of ubiquitinated HDAC7 in this context (Supplemental Figure 4, A and B). Additionally, mutagenesis of serine 155 to alanine on HDAC7 diminished the stabilizing effects of SIK1 (Supplemental Figure 2E), specifically implicating Ser155 as an important residue in HDAC7 stabilization. Previous work has shown that HDAC7 can be stabilized by 14-3-3 proteins in human embryonic kidney (HEK) 293 cells (18). To test whether 14-3-3 protein also participates in HDAC7 stabilization in cardiomyocytes, we infected NRVMs with adenovirus expressing full-length 14-3-3 followed by treatment with the SIK inhibitor YKL-05-099. Overexpression of 14-3-3 increased HDAC7 protein abundance in comparison with empty virus–infected control (Supplemental Figure 4C). However, this effect was lost upon addition of the SIK inhibitor YKL-05-099, suggesting that 14-3-3 proteins may play a role in the stabilization

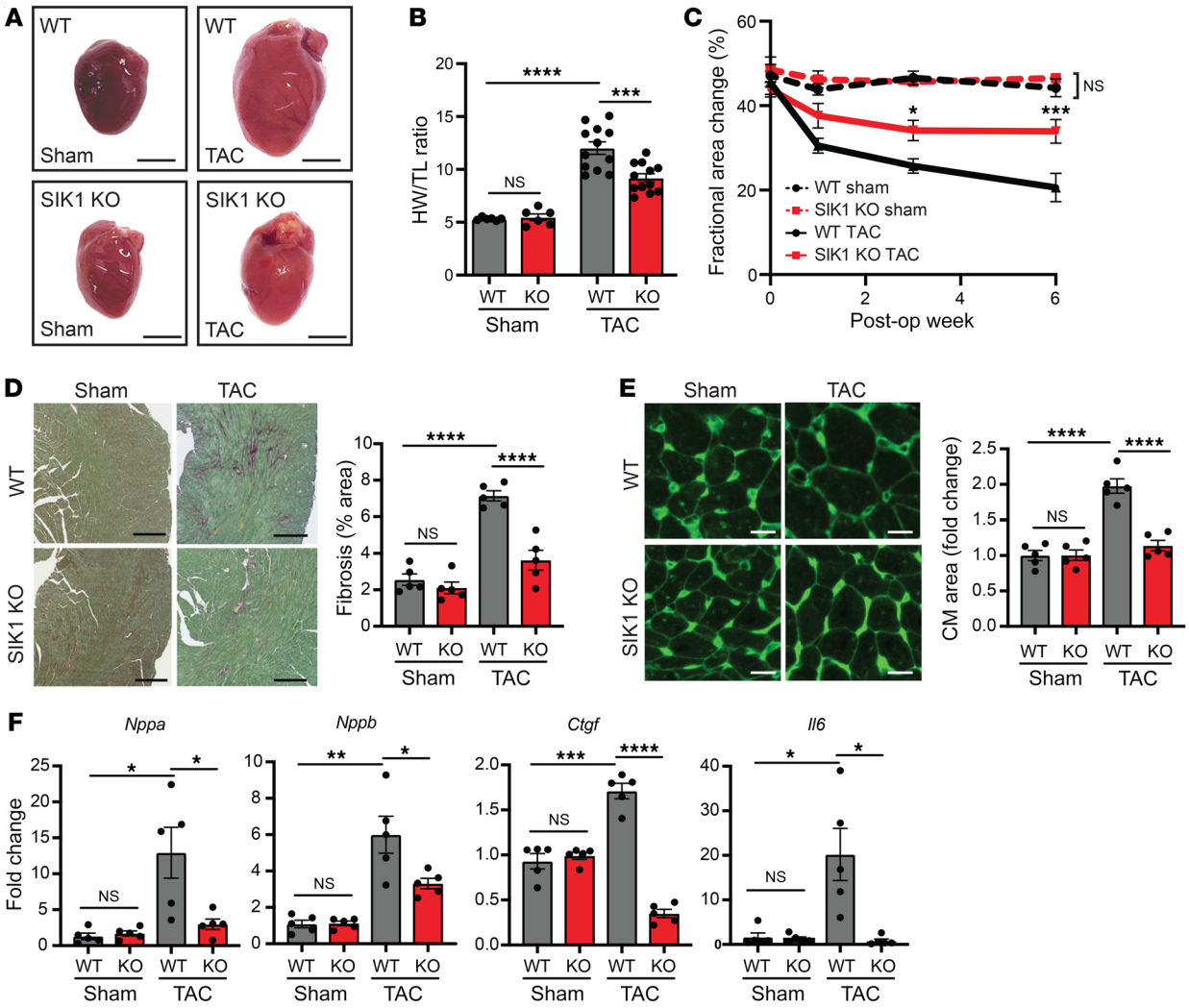

Figure 3. Global loss of SIK1 protects against pathologic cardiac remodeling in vivo. (**A**) Representative photos of freshly excised hearts. Scale bars: 3 mm. (**B**) Heart weight/tibial length (HW/TL) ratio (n = 6 for sham, n = 12 for TAC). (**C**) Echocardiographic measurements of fractional area change (n = 6 for sham, n = 12 for TAC). $^*P < 0.05$, $^{***}P < 0.001$ for SIK1-KO TAC vs. WT TAC by 2-way ANOVA with Tukey's multiple-comparisons test. (**D**) Picrosirius red staining of heart sections (n = 5). Scale bars: 300 μm. (**E**) Wheat germ agglutinin staining of heart sections (n = 5). Scale bars: 20 μm. (**F**) qRT-PCR expression for canonical heart failure–associated genes (n = 5). Data are shown as means ± SEM unless noted. $^*P < 0.05$, $^{**}P < 0.01$, $^{***}P < 0.001$, $^{****}P < 0.0001$, by 1-way ANOVA with Tukey's multiple comparisons test.

of HDAC7, but are dependent on SIK activity to exert their stabilizing effect. Taken together, these results demonstrate that HDAC7 protein abundance in cardiomyocytes is dependent on SIK1 kinase activity and support that direct phosphorylation of HDAC7 by SIK1 is critical for HDAC7 stability.

Loss of HDAC7 protects against pathologic cardiac remodeling. Previous studies of class IIa HDACs in the heart have demonstrated roles for HDAC4, HDAC5, and HDAC9 as MEF2 corepressors that function as negative regulators of cardiomyocyte hypertrophy and the transcriptional response to cardiac stress (2–4). However, to our knowledge, the role of HDAC7 in the heart has not been previously explored. As our data show that SIK1 is a positive regulator of pathologic cardiac remodeling and can stabilize HDAC7, we hypothesized that HDAC7 may also function as a positive regulator of this response, suggesting a role that deviates from the other class IIa HDAC isoforms. We found that siRNA-mediated knockdown of *Hdac7* in NRVMs robustly attenuated PE-induced cardiac hypertrophy and induction of canonical heart failure–related genes (Figure 5, A–C). In contrast, siRNA-mediated knockdown of *Hdac5* led to a robust induction of *Nppa* and *Nppb* transcripts at baseline and after PE stimulation (Figure 5C), consistent with the role of HDAC5 as a transcriptional corepressor. Transduction of a MEF2 reporter construct into NRVMs revealed that *Hdac7* knockdown had no effect on MEF2 transcriptional activity while *Hdac5* knockdown increased MEF2 activity (Figure 5D and Supplemental Figure 4, E and F), further supporting that HDAC7 functions differently from other class IIa HDACs.

We have shown that SIK1 inhibition attenuates cardiomyocyte hypertrophy and heart failure pathogenesis, and is associated with loss of HDAC7 protein abundance. We have also demonstrated that HDAC7 is a positive regulator of cardiomyocyte hypertrophy. To establish a causal link between SIK1 and HDAC7, we tested

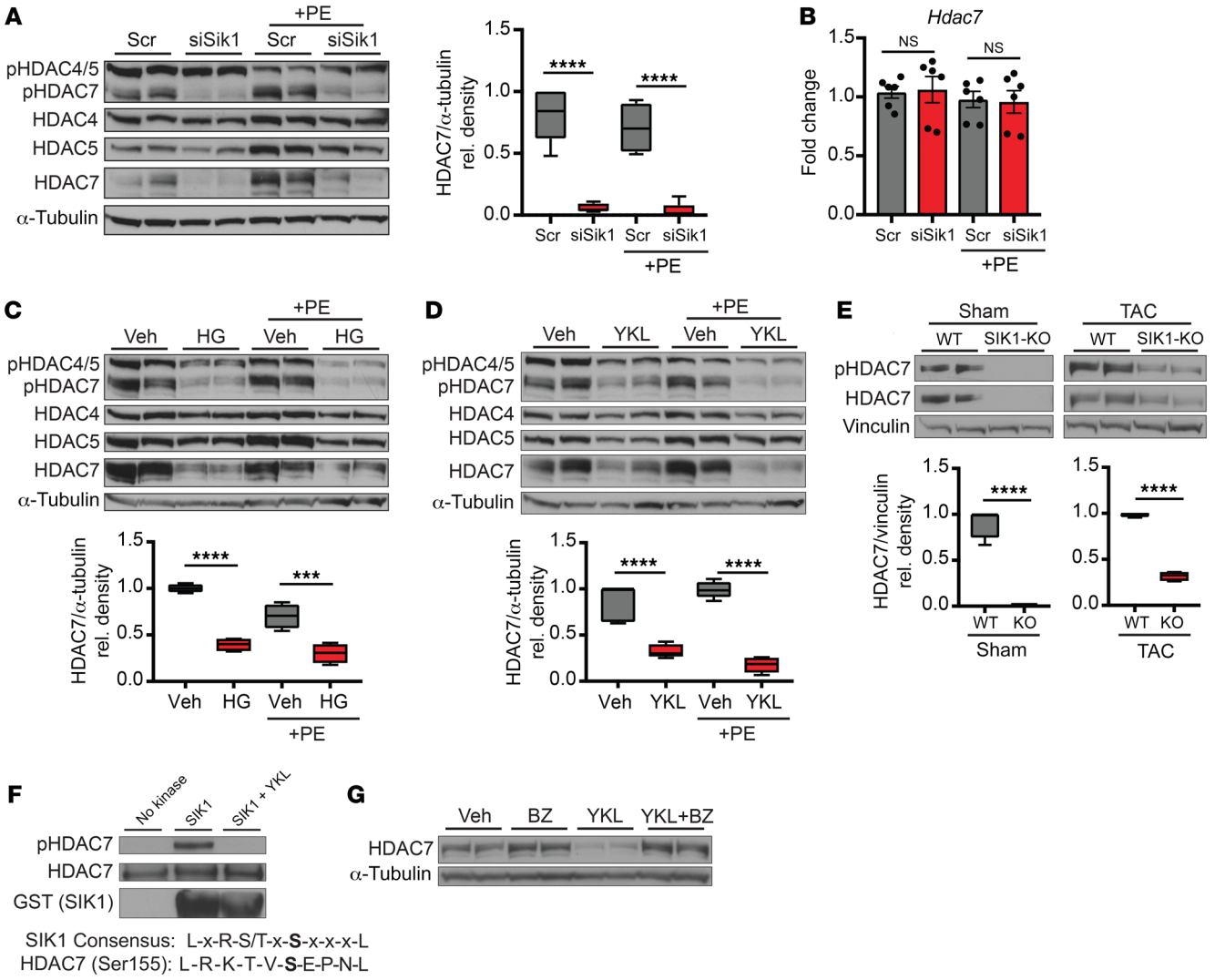

Figure 4. HDAC7 protein stability is dependent on SIK1 kinase activity. (**A**) Western blot for total and phosphorylated HDAC4, HDAC5, and HDAC7 in NRVMs treated with or without siRNA against *Sik1* and with or without PE (100 μM, 24 hours). α-Tubulin was used as loading control ($n = 5$). (**B**) qRT-PCR expression for *Hdac7* ($n = 6$). Bars denote mean ± SEM. (**C** and **D**) Western blot for total and phosphorylated HDAC4, HDAC5, and HDAC7 in NRVMs treated with or without HG-9-91-01 (1 μM) or YKL-05-099 (1 μM). α-Tubulin was used as loading control ($n = 4$). (**E**) Western blot for total and phosphorylated HDAC7 in WT and SIK1-KO sham/TAC LV cardiac tissue. Vinculin was used as loading control ($n = 4$). (**F**) In vitro kinase assay with recombinant HDAC7 and GST-tagged SIK1 plus YKL-05-099 (1 μM). SIK1 consensus sequence is shown below (representative Western blots, $n = 3$). (**G**) Western blot from NRVMs treated with YKL-05-099 (1 μM) and the proteasome inhibitor bortezomib (BZ) (5 nM, 16 hours) (representative Western blots, $n = 3$). All box plots show minimum, maximum, and median with 25th to 75th percentile range. ***$P < 0.001$, ****$P < 0.0001$, by 1-way ANOVA with Tukey's multiple comparisons test.

whether reconstitution of HDAC7 in the setting of SIK1 inhibition would blunt the antihypertrophic effects of SIK1 inhibition. We generated adenoviruses expressing GFP-HDAC7 (Ad-HDAC7) or GFP alone (Ad-GFP) and infected NRVMs, followed by treatment with or without SIK inhibitors and PE. Under nonstimulated conditions, overexpression of HDAC7 was sufficient to induce cardiomyocyte hypertrophy and *Nppa*, *Nppb*, and *Myh7* expression compared with Ad-GFP control (Figure 5, E–G). SIK inhibition inhibited cardiomyocyte hypertrophy (Figure 5, E–G) and depleted HDAC7 protein abundance (Supplemental Figure 3A). Reconstitution of HDAC7 (Western blot of HDAC7 reconstitution shown in Supplemental Figure 3B) partially reversed the protective effects of SIK inhibition during PE-mediated stress (Figures 5, E–G). To test the converse, we infected NRVMs with an adenovirus expressing SIK1 followed by transfection of siRNA probes against *Hdac7*. Overexpression of SIK1 increased *Nppa* and *Nppb* expression in PE-stimulated conditions, but had no appreciable effect at baseline (Supplemental Figure 2, F and G). Knockdown of *Hdac7* robustly attenuated the effect of SIK1 overexpression (Supplemental Figure 2, F and G). These results support a model in which SIK1 promotes cardiomyocyte hypertrophy and stress-gene induction, in part, via activation of HDAC7.

HDAC7 indirectly regulates c-Myc expression. Our data show that HDAC7 is a prohypertrophic transcriptional regulator (Figure 5) and suggest that HDAC7 does not function as a MEF2 corepressor (Figure 5D). These findings support the contention that HDAC7 functions differently from other class IIa HDACs. Emerging studies have described noncanonical roles for HDAC7 in oth-

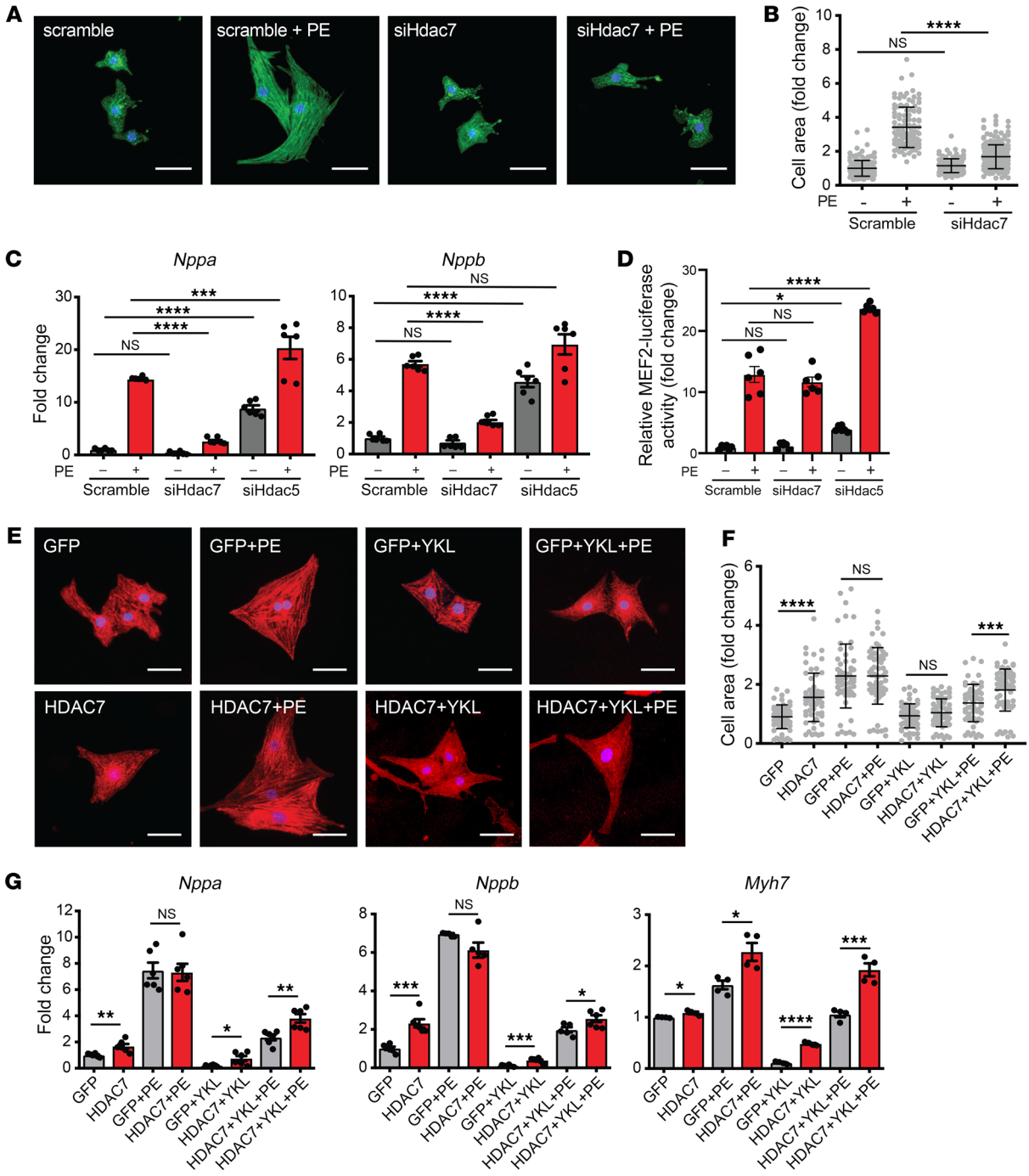

Figure 5. Loss of HDAC7 protects against pathologic cardiac remodeling in vitro. (**A**) NRVMs treated with siRNA against *Hdac7* and immunostained for α-actinin (green) and nuclei (blue). Scale bars: 40 μm. (**B**) Cell area of NRVMs (n = 108). Bars denote mean ± SD. (**C**) qRT-PCR expression for *Nppa* and *Nppb* (n = 6). (**D**) MEF2 dual luciferase reporter assay. Values were normalized to Renilla luciferase control (n = 6). (**E**) NRVMs infected with adenovirus harboring GFP-HDAC7 or GFP alone and immunostained for α-actinin (red) and nuclei (blue). Scale bars: 40 μm. (**F**) Cell area of NRVMs (n = 58–63). Bars denote mean ± SD. (**G**) qRT-PCR expression for canonical heart failure–associated genes (n = 6). Data are shown as means ± SEM unless noted. *P < 0.05, **P < 0.01, ***P < 0.001, ****P < 0.0001, by 1-way ANOVA with Tukey's multiple comparisons test.

er biological contexts, including a role as an activator of *c-Myc* in cancer (19). Given the importance of *c-Myc* in establishing pathologic remodeling in the heart (7, 8, 20), we tested whether *c-Myc* expression was altered with HDAC7 perturbation in cardiomyocytes. Silencing of *Hdac7* led to a decrease in *c-Myc* RNA and robustly depleted C-MYC protein in NRVMs (Figure 6, A and B). Conversely, overexpression of HDAC7 induced *c-Myc* expression at both the RNA and protein levels (Figure 6, C and D). Similarly, treatment with the SIK inhibitor YKL-05-099, which robustly depletes HDAC7 (Figure 4D), led to a marked decrease in *c-Myc* mRNA and protein expression (Figure 6, E and F). Cardiac tissue samples from SIK1 KO mice also exhibited lower *c-Myc* RNA and

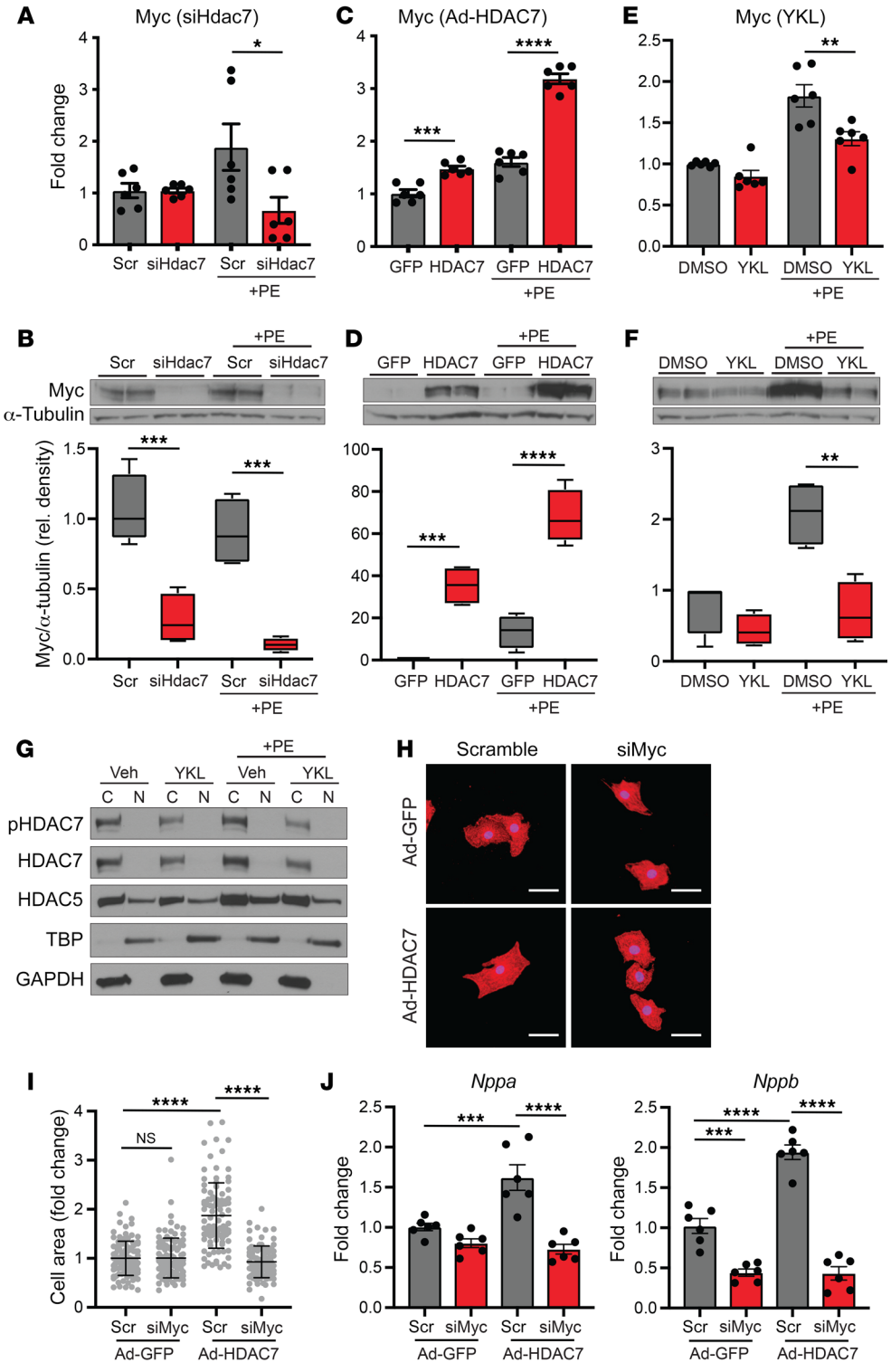

Figure 6. HDAC7 indirectly regulates c-Myc expression. qRT-PCR (n = 6) and Western blotting (n = 4) for c-Myc expression in NRVMs treated with siRNA against *Hdac7* (**A** and **B**), Ad-HDAC7 (**C** and **D**), or YKL-05-099 (1 μM) (**E** and **F**). All box plots show minimum, maximum, and median with 25th to 75th percentile range. (**G**) Western blotting of cytoplasmic (C) and nuclear (N) fractions of NRVMs treated with 1 μM YKL-05-099 plus 100 μM PE. TATA box–binding protein (TBP) and GAPDH were used as nuclear and cytoplasmic markers, respectively (representative Western blots, n = 3). (**H**) NRVMs treated with adenovirus harboring GFP-HDAC7 or GFP alone, followed by transfection of siRNA probes against *c-Myc* or scramble control. Immunostained for α-actinin (red) and nuclei (blue). Scale bars: 40 μm. (**I**) Cell area of NRVMs (n = 100). Bars denote mean ± SD. (**J**) qRT-PCR expression for *Nppa* and *Nppb* (n = 6). Data are shown as means ± SEM unless noted. $^*P < 0.05$, $^{**}P < 0.01$, $^{***}P < 0.001$, $^{****}P < 0.0001$, by 1-way ANOVA with Tukey's multiple comparisons test.

protein expression levels compared with WT control mice (Supplemental Figure 3, D and E).

To determine whether HDAC7 directly or indirectly regulates *c-Myc* expression, we first assessed the nuclear/cytoplasmic distribution of HDAC7 in NRVMs. Other class IIa HDACs have been shown to shuttle between the nuclear and cytoplasmic compartments, and it is thought that control of their spatial localization is a central mechanism for regulating their function. We performed nuclear/cytoplasmic fractionation on NRVM lysates treated with the SIK inhibitor YKL-05-099 with or without PE stimulation. Under all conditions, total and phosphorylated HDAC7 protein was found exclusively in the cytoplasmic fraction and was notably absent in the nuclear fraction (Figure 6G). Treatment of NRVMs with the proteasome inhibitor bortezomib, which causes accumulation of HDAC7 protein, also did not reveal any detectable levels of HDAC7 protein in the nuclear fraction (Supplemental Figure

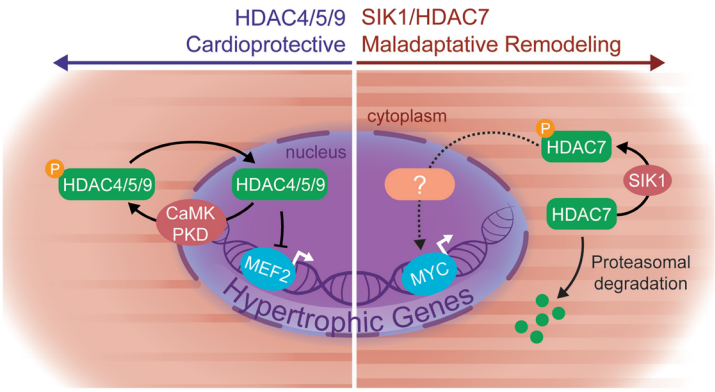

Figure 7. Proposed working model. Our proposed working model implicates a prohypertrophic SIK1/HDAC7 signaling axis in cardiac myocytes and a departure from the canonical model of class IIa HDAC function.

3C). In contrast, HDAC5 protein was detected in both nuclear and cytoplasmic fractions as previously reported (Figure 6G, Supplemental Figure 3C, and ref. 21). The lack of detectable HDAC7 in the nuclear fraction of NRVMs indicates that HDAC7 is unlikely to regulate *c-Myc* expression via direct enrichment on DNA regulatory elements in cardiomyocytes.

Overexpression of HDAC7 in NRVMs induces hypertrophy and *c-Myc* expression (Figure 5, E–G, and Figure 6, C and D). To test whether HDAC7-mediated hypertrophy is dependent on *c-Myc* induction, we infected NRVMs with Ad-HDAC7 followed by transfection of siRNA probes against *c-Myc* (Supplemental Figure 3, F and G). *c-Myc* knockdown had no effect on cell size in empty virus–infected NRVMs, but attenuated HDAC7-induced cardiomyocyte hypertrophy and *Nppa* and *Nppb* expression (Figure 6, H–J). Taken together, these data indicate that HDAC7 acts as a positive upstream regulator of C-MYC during cardiomyocyte hypertrophy, further suggesting that the SIK1/HDAC7 axis functions in a manner that is different from the signal-responsive MEF2 corepressor role of related class IIa HDAC isoforms.

Discussion

Our results implicate the SIK family of kinases as key regulators of cardiac plasticity in rodent models and human cardiomyocytes, significantly expanding our fundamental understanding of how stress signaling cascades are coupled to the cardiomyocyte gene regulatory machinery. In contrast to previously known cardiac class IIa HDAC kinases such as CaMKII and PKD, which function primarily via HDAC nuclear-cytoplasmic shuttling, we establish an apparently unique role for SIK1 as a critical effector of HDAC7 stabilization. Our data demonstrate a mechanistic link between SIK1 and HDAC7, implicate this axis as part of a prohypertrophic signaling node, and provide new insights into the function of HDAC7 — one of the least well characterized HDAC family members in cardiac biology (Figure 7, summary diagram).

SIK1 mediates HDAC7 stability. Established cardiac class IIa HDAC kinases in the heart, such as CaMK and protein kinase C/D (21–23), directly phosphorylate class IIa HDACs, leading to their nuclear export and subsequent derepression of MEF2 transcriptional activity. In contrast, our data on SIK1 support a differentiated mode of regulation that uncovers a new layer of control at the level of HDAC7 protein stabilization. In the heart, SIK1-mediated stabilization of HDAC7 is robust and appears to be specific for HDAC7 over other class IIa family members. Why HDAC7 stability is particularly sensitive to SIK1 inhibition is unclear, especially in light of the fact that other class IIa HDAC kinases (CaMK, PKD) can phosphorylate similar epitopes. Previous studies have shown that CaMKII signals exclusively to HDAC4 through a unique CaMKII docking sequence present only on HDAC4 and is absent in other class IIa HDACs (23). It is possible that the specificity of SIK1 signaling could be achieved through a similar docking domain within HDAC7.

How exactly SIK1-mediated phosphorylation of HDAC7 promotes increased HDAC7 stability also remains unclear. Our data implicate Ser155 on HDAC7 as an important determinant of SIK1-mediated stabilization, although other serine residues may also play a role in this process. We speculate that phosphorylated HDAC7 may have increased affinity for binding to 14-3-3 proteins, protecting HDAC7 from targeted proteasomal degradation, as has been suggested from previous studies in HEK293 cells (18). In support of this mechanism, we find that overexpression of 14-3-3 in NRVMs can increase HDAC7 protein abundance. Our observation that this stabilizing effect of 14-3-3 overexpression is abrogated by SIK inhibition suggests a model in which SIK-mediated phosphorylation of HDAC7 is a dominant trigger for protein stabilization, while 14-3-3 further facilitates the protection of HDAC7 from the protein degradation machinery. Although our study identifies HDAC7 as an important downstream target of SIK1 activity, additional substrates of SIK1 signaling likely play a role in cardiac remodeling. Future studies leveraging unbiased approaches, such as phospho-proteomics, may identify additional downstream effectors of SIK1 signaling that participate in cardiac homeostasis and stress responses.

HDAC7 is a prohypertrophic HDAC. The contention that class IIa HDACs in the heart function primarily as transcriptional corepressors of MEF2 is derived from studies focused exclusively on HDAC4, HDAC5, and HDAC9. This prior work has shown that loss of function of these HDACs leads to excessive MEF2 activity and heart failure (2, 3), consistent with the role of these HDAC isoforms as transcriptional repressors and negative regulators of cardiomyocyte hypertrophy. In contrast, the role of HDAC7 in the heart has been largely unexplored. Using cultured cardiomyocytes, we find that HDAC7 functions as a positive regulator of cardiomyocyte hypertrophy, suggesting major mechanistic differences from the other class IIa HDACs. Recent studies have demonstrated highly specific roles of HDAC4 signaling, including the identification of a proteolytically cleaved N-terminal fragment of HDAC4, suggesting that significant functional specificity exists even between proteins as closely related as HDAC4 and HDAC5 (4, 24). Consistent with this deviation in function, we also find that HDAC7 can strongly induce *c-Myc* expression — a robust and established driver of stress-dependent cardiac gene expression and pathologic remodeling. Surprisingly, we find that HDAC7 resides exclusively in the cytoplasm of NRVMs and is notably absent in the nuclear compartment. It will be important to understand the precise mechanisms by which HDAC7 regulates *c-Myc*

expression, as such regulation is unlikely to involve direct enrichment of HDAC7 on *c-Myc* regulatory loci in cardiomyocytes. The absence of detectable HDAC7 in the cardiomyocyte nucleus implicates that class IIa HDACs may have many functions outside of direct regulation of gene expression (19, 25–27). Further studies to explore the HDAC7-dependent transcriptome and protein interactome in cardiomyocytes will shed important light on the detailed mechanisms of HDAC7 function.

The role of SIK1 in nonmyocyte cells. Our studies using chemical probes and siRNAs in cultured cardiomyocytes support a cell-autonomous role for SIK1 in these tissues. Although we have shown that SIK1-null mice are protected from pressure overload–induced heart failure, it remains possible that SIK1 expression in non-cardiomyocyte cell types is influencing the phenotype in vivo. Similar to our observations in cultured cardiomyocytes, we find that the hearts of SIK1-null mice are depleted in HDAC7 protein, implicating that the SIK1/HDAC7 axis in cardiomyocytes is also operative in vivo. Silencing of HDAC7 has also been shown to inhibit myofibroblast differentiation (28), suggesting that SIK1 expression in fibroblasts may also contribute to heart failure pathogenesis. Although our current work establishes a role for SIKs in heart failure pathobiology, in the future it will be informative to annotate the role of SIK1 in other relevant cellular compartments that populate the stressed myocardium using a conditional gene-deletion approach.

In summary, we show that SIK1 is a previously unrecognized effector of stress-mediated hypertrophic remodeling and gene induction in rodent and human cardiomyocytes, in part through its ability to regulate HDAC7 protein stability. We establish an apparently new role for HDAC7 as a prohypertrophic effector, a target of SIK1, and an upstream regulator of *c-Myc* expression in cardiomyocytes, reflecting functions that are distinct from those of related class IIa HDAC family members. Our findings in rodent models and human iPSC–derived cardiomyocytes suggest that interdicting the SIK1/HDAC7 signaling cascade may be a therapeutic approach in human heart failure.

Methods

NRVM isolation and culture. NRVMs were isolated from hearts of 2-day-old Sprague-Dawley rat pups (Charles River) under aseptic conditions as previously described (29). Cells were preplated for 2 hours on tissue culture plates followed by 48 hours of exposure to BrdU in culture medium to remove contaminating nonmyocytes. NRVMs were plated in growth medium (DMEM, 5% FBS, 100 U/mL penicillin-streptomycin) for 48 hours and switched to serum-free medium thereafter (DMEM, 0.1% BSA, 1% insulin-transferring selenium, 100 U/mL penicillin-streptomycin). Before stimulation with PE, NRVMs were maintained in serum-free medium for 48–72 hours. NRVMs were treated with SIK inhibitors at the indicated concentrations for 16 hours before PE stimulation (100 μM). For siRNA treatments, NRVMs were transfected with RNAiMax (Invitrogen) and 50 nM of siRNA in serum-free medium for 48 hours before PE stimulation (100 μM). siRNAs were purchased from Sigma-Aldrich (scramble control siRNA, SIC001; *Sik1* siRNA, SASI_Rn01_00053040; *Sik3* siRNA, SASI_Rn02_00326476; *Hdac5* siRNA, SASI_Rn02_00372147; *Hdac7* siRNA, SASI_Rn02_00277288; *c-Myc* siRNA, SASI_Rn01_00089127).

Western blotting. To prepare whole cell extracts, NRVMs were lysed in RIPA buffer supplemented with protease and phosphatase inhibitors (Roche). Protein concentrations were quantified by BCA assay (Thermo Fisher Scientific, 23225). Lysates were diluted in 4× reducing Laemmli buffer, boiled at 95°C for 5 minutes, and resolved on a 4%–12% Bis-Tris SDS-PAGE gel. Resolved proteins were transferred onto a PVDF membrane. Membranes were then blocked with 5% milk in TBST for 1 hour at room temperature followed by primary antibody incubation overnight at 1:1000 dilution in 5% BSA or milk. After overnight incubation, secondary HRP-conjugated antibody was added for 1 hour at a dilution of 1:1000 to 1:5000 in 5% milk in TBST. Membranes were incubated with Amersham ECL Prime Western Blotting Detection Reagent (GE Life Sciences, RPN2232) and exposed to autoradiography film at various time intervals.

Catalog numbers for antibodies used in this study were as follows: phospho-HDAC4(Ser246)/HDAC5(Ser259)/HDAC7(Ser155) (Cell Signaling Technology [CST], 3443), phospho-HDAC4(Ser632)/HDAC5 (Ser661)/HDAC7(Ser486) (CST, 3424), phospho-HDAC7(Ser318) (Novus Biologicals, NBP2-03978), HDAC4 (CST, 7628), HDAC5 (CST, 20458), HDAC7 (CST, 33418), α-tubulin (Sigma-Aldrich, 05829), vinculin (Sigma-Aldrich, V9131), c-Myc (CST, 5605), GST (CST, 2625), SIK3 (MRC Protein Phosphorylation and Ubiquitylation Unit, DU39537), 14-3-3 (CST, 8312), GAPDH (CST, 5174), TBP (Abcam, ab51841).

qRT-PCR from NRVMs and mouse tissue. Total RNA was extracted from NRVMs using the High Pure RNA Isolation Kit (Roche) according to the manufacturer's instructions. For cardiac tissue, a 10- to 20-mg piece of mouse LV tissue was collected and preserved in RNAlater (Qiagen) followed by mechanical disruption/homogenization in PureZOL (Bio-Rad) on a TissueLyser II (Qiagen). The RNA containing aqueous phase was extracted with chloroform and further purified using the Aurum Total RNA Fatty and Fibrous Tissue Kit (Bio-Rad). First-strand cDNA synthesis was performed using iScript Reverse Transcription Supermix (Bio-Rad). TaqMan-based qRT-PCR was performed using SsoAdvanced Universal Probes Supermix (Bio-Rad), labeled probes from the Universal Probe Library (Roche), and gene-specific oligonucleotide primers on a CFX384 Touch Real-Time PCR Detection System (Bio-Rad). A list of qRT-PCR primers and a list of TaqMan probes are provided in Supplemental Tables 1 and 2, respectively. Relative expression was calculated using the $2^{\Delta\Delta Ct}$ method with normalization to *Ppib*.

Mouse model of cardiac hypertrophy and heart failure. All mice were aged 8–10 weeks before surgery. Sham and TAC surgeries were performed as previously described (29). Briefly, mice were anesthetized with isoflurane, mechanically ventilated, and subjected to thoracotomy. For TAC surgery, the aortic arch was constricted between the left common carotid and the brachiocephalic arteries using a 7-0 silk suture and a 25-gauge needle. In sham surgeries, thoracotomy was performed as above, and the aorta was surgically exposed without further intervention.

Transthoracic echocardiography. Mice were anesthetized with 1% inhalational isoflurane and imaged using the Vevo 770 High Resolution Imaging System (Fujifilm VisualSonics Inc.) and the RMV-707B 30-MHz probe. Measurements were obtained from M-mode sampling and integrated electrocardiogram-gated kilohertz visualization (EKV) images taken in the LV short axis view at the mid–papillary muscle level as previously described (29).

Histology and immunofluorescence. For cellular immunofluorescence studies, NRVMs were seeded on glass coverslips coated with 0.1% gelatin. NRVMs were fixed in 2% paraformaldehyde for 20 min-

utes at room temperature followed by permeabilization with PBST plus 0.1% Triton X. NRVMs were incubated in PBST plus 5% horse serum for 1 hour and then stained with primary antibody against α-actinin at 1:800 (Sigma-Aldrich, A7811) for 1 hour. NRVMs were washed 3 times with PBST followed by staining with secondary antibody at 1:1000 for 1 hour. Cells were washed 3 times with PBST and mounted with Vectashield Hardset mounting medium with DAPI. For cardiac tissue samples, mid-ventricular short axis cross sections were fixed in 10% neutral-buffered formalin overnight at 4°C and transferred to 100% ethanol for 24 hours. Samples were embedded in paraffin blocks, sectioned, and stained with Picrosirius red (Polysciences) or Wheat Germ Agglutinin 488 (Thermo Fisher Scientific, W11261) according to the manufacturers' instructions. Fibrosis area and cardiomyocyte cross-sectional area were quantified as previously described (29).

Luciferase assay. NRVMs were infected with adenovirus harboring MEF2 firefly luciferase and Renilla luciferase (Seven Hills Bioreagents) at an MOI of 1 for 2 hours, followed by PBS wash and culture in serum-free medium. Twenty-four hours after infection, NRVMs were transfected with siRNAs against *Hdac5*, *Hdac7*, or scramble control. Forty-eight hours after siRNA transfection, cells were then treated with PE (100 μM) for 48 hours and harvested using the Dual Luciferase Reporter Assay (Promega) according to the manufacturer's instructions. MEF2 luciferase reporter values were normalized to internal Renilla luciferase signal.

Adenovirus. Adenoviruses were generated by cloning of target fragments into the Gateway entry vector pENTR2B, followed by LR recombination into Gateway destination vector pAd-CMV-V5 DEST and transfection into 293A cells according to the manufacturer's protocol. The GFP-HDAC7 plasmid was provided by Jeroen Roose (UCSF). Cell plaques were observed as early as 1 week after transfection and were fully lysed no later than 2 weeks after transfection. 293A cells were then infected with serially diluted crude adenoviral lysate and overlaid with SeaPlaque Agarose to allow for plaque formation. Single plaques were isolated and tested for protein expression. Validated plaques were amplified on 293A cells and titered using a standard plaque formation assay to calculate plaque-forming units (PFU). Ad-14-3-3 and Ad-SIK1 viruses were purchased from Vector Biolabs. To infect NRVMs, cells were incubated in low volume of serum-free medium containing adenoviral particles (MOI of 1) for 2 hours in 37°C 5% CO_2 with rocking every 30 minutes. NRVMs were washed with PBS without Ca^{2+} or Mg^{2+} and cultured in fresh serum-free medium.

qRT-PCR and BNP ELISA from iPSC cardiomyocytes. iPSC cardiomyocytes were purchased from Cellular Dynamics and maintained according to the manufacturer's protocols. Cells were seeded on 96-well culture plates coated with 5 μg/mL of fibronectin and maintained in Williams' E Medium supplemented with 1:25 of Cell Maintenance Cocktail B (Thermo Fisher Scientific, CM4000). For hypertrophic stimulation, cells were pretreated with SIK inhibitors for 16 hours, followed by stimulation with 10 nM of endothelin-1 (ET-1) for 18 hours. RNA was isolated and reverse-transcribed using the TaqMan Cells-to-CT kit (Life Technologies, AM1278) according to the manufacturer's instructions. qRT-PCR was performed using Life Technologies TaqMan assays for human *NPPB* and *B2M* (housekeeping) (*NPPB*, Hs00173590_m1; *B2M*, Hs000984230_m1). ELISA for BNP protein was performed using 6 μL of spent medium from each well of a 96-well plate as previously described (29) with the following antibodies: anti-proBNP capture antibody (Abcam, ab13111), anti-proBNP detection antibody (Abcam, ab13124), and N-terminal proBNP peptide standard (Phoenix Pharmaceuticals, 011-42).

Cell area measurements for iPSC cardiomyocytes. For cell size assays, cells were plated on Ibidi 8-well chamber slides and pretreated with SIK inhibitors for 16 hours, followed by stimulation with 10 nM ET-1 (Sigma-Aldrich, E7764) for 18 hours. Cells were fixed in 2% paraformaldehyde for 20 minutes, permeabilized with PBST plus 0.1% Triton X-100 for 20 minutes, and blocked with PBST plus 5% horse serum for 1 hour at room temperature. Primary antibody against sarcomeric α-actinin was used at a dilution of 1:800 in PBST plus 5% horse serum for 1 hour at room temperature. Secondary anti-mouse antibody was used at a dilution of 1:1000 in PBST plus 5% horse serum for 1 hour at room temperature. Cells were imaged and quantified as previously described (29).

In vitro kinase assay. Ten nanograms of recombinant SIK1 (Thermo Fisher Scientific) and 100 ng of recombinant HDAC7 (Origene) were incubated in a final volume of 40 μL containing 1× kinase buffer (CST) supplemented with 100 μM ATP. One micromolar YKL-05-099 was added for inhibition of SIK1 activity. Reactions were incubated for 30 minutes at 30°C, followed by addition of 4× Laemmli buffer. Samples were boiled at 95°C for 5 minutes and resolved by SDS-PAGE.

Nuclear/cytoplasmic fractionation. Nuclear and cytoplasmic fractions were prepared from NRVMs using the NE-PER Nuclear and Cytoplasmic Extraction Reagents (Thermo Fisher Scientific, 78833) according to the manufacturer's instructions.

Statistics. Data were evaluated by 1-way and 2-way ANOVA with Tukey's multiple-comparisons test. Differences with a P value less than or equal to 0.05 were considered statistically significant.

Study approval. All protocols concerning animal use were approved by the Institutional Animal Care and Use Committees at the University of California, San Francisco, and conducted in strict accordance with the NIH *Guide for the Care and Use of Laboratory Animals* (National Academies Press, 2011). Mice were housed in a temperature- and humidity-controlled pathogen-free facility on a 12-hour light/12-hour dark cycle with ad libitum access to water and standard laboratory rodent chow.

Author contributions

AH designed the study, conducted experiments, performed echocardiography, analyzed data, and wrote the manuscript. QD performed biochemical experiments and echocardiography. SM performed iPSC experiments. YH performed animal surgeries and echocardiography. SABW performed genotyping of mice, and NSG and BW provided expertise and advisement. BGB provided expertise, advisement, and critical revisions to the manuscript. SMH designed the study and provided expertise, advisement, and critical revisions to the manuscript.

Acknowledgments

We thank members of the Bruneau laboratory, Gladstone Stem Cell Core, Gladstone Histology and Light Microscopy Core, and the Gladstone Animal Facility for their technical expertise; Tim McKinsey (University of Colorado Denver) and Tianjing Hu (University of Colorado Denver) for their advice and technical expertise in generating adenovirus; Brian Black (UCSF) for discussion and critical input; Ana Silva (ana@anasilvaillustrations.com) for expert assistance with graphical design; and Jeroen Roose for the GFP-HDAC7 plasmid. AH was supported by a predoctoral fellowship

from the Tobacco-Related Disease Research Program (28DT-008), the UCSF Discovery Fellows Program, an Achievement Rewards for College Scientists Scholarship, and NIH grant T32GM008568. SM was supported by a predoctoral fellowship from the American Heart Association (17PRE33670181) and the UCSF Discovery Fellows Program. BGB acknowledges support from the Gladstone Institutes and the Younger Family Fund. SMH was supported by NIH HL127240 and the Gladstone Institutes. This work was also supported by an NIH/National Center for Research Resources grant (C06 RR018928) to the Gladstone Institutes.

Address correspondence to: Saptarsi M. Haldar, Amgen Research, 1120 Veterans Boulevard, South San Francisco, California 94080, USA. Phone: 650.244.2561; Email: shalda01@amgen.com, saptarsi.haldar@gladstone.ucsf.edu. Or to: Benoit G. Bruneau, Gladstone Institute of Cardiovascular Disease, 1650 Owens Street, San Francisco, California 94158, USA. Phone: 415.734.7400; Email: benoit.bruneau@gladstone.ucsf.edu.

SMH's present address is: Amgen Research, South San Francisco, California, USA.

1. Hill JA, Olson EN. Cardiac plasticity. *N Engl J Med*. 2008;358(13):1370–1380.
2. Zhang CL, McKinsey TA, Chang S, Antos CL, Hill JA, Olson EN. Class II histone deacetylases act as signal-responsive repressors of cardiac hypertrophy. *Cell*. 2002;110(4):479–488.
3. Chang S, McKinsey TA, Zhang CL, Richardson JA, Hill JA, Olson EN. Histone deacetylases 5 and 9 govern responsiveness of the heart to a subset of stress signals and play redundant roles in heart development. *Mol Cell Biol*. 2004;24(19):8467–8476.
4. Lehmann LH, et al. A proteolytic fragment of histone deacetylase 4 protects the heart from failure by regulating the hexosamine biosynthetic pathway. *Nat Med*. 2018;24(1):62–72.
5. Berdeaux R, et al. SIK1 is a class II HDAC kinase that promotes survival of skeletal myocytes. *Nat Med*. 2007;13(5):597–603.
6. Wang B, et al. A hormone-dependent module regulating energy balance. *Cell*. 2011;145(4):596–606.
7. Jackson T, Allard MF, Sreenan CM, Doss LK, Bishop SP, Swain JL. The c-myc proto-oncogene regulates cardiac development in transgenic mice. *Mol Cell Biol*. 1990;10(7):3709–3716.
8. Ahuja P, et al. Myc controls transcriptional regulation of cardiac metabolism and mitochondrial biogenesis in response to pathological stress in mice. *J Clin Invest*. 2010;120(5):1494–1505.
9. Simpson P, McGrath A, Savion S. Myocyte hypertrophy in neonatal rat heart cultures and its regulation by serum and by catecholamines. *Circ Res*. 1982;51(6):787–801.
10. Sundberg TB, et al. Development of chemical probes for investigation of salt-inducible kinase function in vivo. *ACS Chem Biol*. 2016;11(8):2105–2111.
11. Chen HH, Burnett JC. Natriuretic peptides in the pathophysiology of congestive heart failure. *Curr Cardiol Rep*. 2000;2(3):198–205.
12. Sugden PH, Clerk A. Cellular mechanisms of cardiac hypertrophy. *J Mol Med*. 1998;76(11):725–746.
13. Zhi D, et al. Whole-exome sequencing and an iPSC-derived cardiomyocyte model provides a powerful platform for gene discovery in left ventricular hypertrophy. *Front Genet*. 2012;3:92.
14. Wein MN, Foretz M, Fisher DE, Xavier RJ, Kronenberg HM. Salt-inducible kinases: physiology, regulation by cAMP, and therapeutic potential. *Trends Endocrinol Metab*. 2018;29(10):723–735.
15. Paulo E, et al. Sympathetic inputs regulate adaptive thermogenesis in brown adipose tissue through cAMP-Salt inducible kinase axis. *Sci Rep*. 2018;8(1):11001.
16. Rockman HA, et al. Segregation of atrial-specific and inducible expression of an atrial natriuretic factor transgene in an in vivo murine model of cardiac hypertrophy. *Proc Natl Acad Sci U S A*. 1991;88(18):8277–8281.
17. Kao HY, Verdel A, Tsai CC, Simon C, Juguilon H, Khochbin S. Mechanism for nucleocytoplasmic shuttling of histone deacetylase 7. *J Biol Chem*. 2001;276(50):47496–47507.
18. Li X, Song S, Liu Y, Ko SH, Kao HY. Phosphorylation of the histone deacetylase 7 modulates its stability and association with 14-3-3 proteins. *J Biol Chem*. 2004;279(33):34201–34208.
19. Zhu C, et al. The role of histone deacetylase 7 (HDAC7) in cancer cell proliferation: regulation on c-Myc. *J Mol Med*. 2011;89(3):279–289.
20. Starksen NF, et al. Cardiac myocyte hypertrophy is associated with c-myc protooncogene expression. *Proc Natl Acad Sci U S A*. 1986;83(21):8348–8350.
21. Vega RB, et al. Protein kinases C and D mediate agonist-dependent cardiac hypertrophy through nuclear export of histone deacetylase 5. *Mol Cell Biol*. 2004;24(19):8374–8385.
22. Harrison BC, et al. Regulation of cardiac stress signaling by protein kinase d1. *Mol Cell Biol*. 2006;26(10):3875–3888.
23. Backs J, Song K, Bezprozvannaya S, Chang S, Olson EN. CaM kinase II selectively signals to histone deacetylase 4 during cardiomyocyte hypertrophy. *J Clin Invest*. 2006;116(7):1853–1864.
24. Backs J, et al. Selective repression of MEF2 activity by PKA-dependent proteolysis of HDAC4. *J Cell Biol*. 2011;195(3):403–415.
25. Salian-Mehta S, Xu M, McKinsey TA, Tobet S, Wierman ME. Novel interaction of class IIb histone deacetylase 6 (HDAC6) with class IIa HDAC9 controls gonadotropin releasing hormone (GnRH) neuronal cell survival and movement. *J Biol Chem*. 2015;290(22):14045–14056.
26. Bakin RE, Jung MO. Cytoplasmic sequestration of HDAC7 from mitochondrial and nuclear compartments upon initiation of apoptosis. *J Biol Chem*. 2004;279(49):51218–51225.
27. Gupta MP, Samant SA, Smith SH, Shroff SG. HDAC4 and PCAF bind to cardiac sarcomeres and play a role in regulating myofilament contractile activity. *J Biol Chem*. 2008;283(15):10135–10146.
28. Kang DH, et al. Silencing histone deacetylase 7 alleviates transforming growth factor-β1-induced profibrotic responses in fibroblasts derived from Peyronie's plaque. *World J Mens Health*. 2018;36(2):139–146.
29. Duan Q, et al. BET bromodomain inhibition suppresses innate inflammatory and profibrotic transcriptional networks in heart failure. *Sci Transl Med*. 2017;9(390):eaah5084.